13th World Conference on Earthquake Engineering
Vancouver, B.C., Canada
August 1-6, 2004
Paper No. 3401

CONTROLLABLE FRICTION DAMPER USING PIEZOELECTRIC ACTUATORS FOR SEMI-ACTIVE SEISMIC ISOLATION SYSTEM

Eiji SATO[1], Takafumi FUJITA[2]

SUMMARY

A semi-active seismic isolation system using a controllable friction damper was developed to decrease the relative displacement between the ground and a superstructure. Performance of the controllable friction damper is hampered, however, when the controller and the actuator malfunction during a large earthquake. In this study, a new controllable friction damper, using dependable piezoelectric actuators, is proposed as a solution. This damper has a fail-safe mechanism enabling the system to demonstrate a damping effect during malfunctions. This paper outlines the simulation results for the seismic isolation effect, and the relative displacement reduction effect of a semi-active seismic isolation system using the controllable friction damper, and also reports the results of excitation tests for a semi-active seismic isolation system using this controllable friction damper.

INTRODUCTION

To decrease response acceleration of superstructures during an earthquake, several base-isolated buildings have been constructed using passive isolation systems [1]. The trade-off is that large relative displacement is inevitable in the passive seismic isolation system in order to decrease the response acceleration of the superstructures.

To solve this trade-off problem, a semi-active seismic isolation system using a controllable friction damper was developed in which the damping force was controlled by varying the pressure between the friction materials [2,3]. However, if the controller and the actuators, which press the friction material, malfunction, the damping force cannot be generated at all.

To solve this problem, a new controllable friction damper with a fail-safe mechanism is produced. To simplify the mechanism, dependable piezoelectric actuators, that are compact, can generate a large force and respond quick, are used. Simulations of the semi-active seismic isolation system with this controllable friction damper are performed to examine the seismic isolation and the relative displacement reduction. Several experiments are conducted to obtain characteristics of this controllable friction damper. A numerical model of the controllable friction damper is developed using the results of these experiments.

[1] Researcher, National Research Institute for Earth Science and Disaster Prevention, Japan
[2] Professor, Institute of Industrial Science, The University of Tokyo, Japan

The semi-active controller is designed by two control methods. To establish the semi-active isolation and the relative displacement reduction, shaking table tests for the semi-active isolation system with this damper are conducted. This paper describes the results of the simulations and the experiments.

FUNDAMENTAL ANALYSIS FOR SEMI-ACTIVE SEISMIC ISOLATION SYSTEM WITH CONTROLLABLE FRICTION DAMPER

Controllable friction damper

A controllable friction damper of the conventional system, (hereafter referred to as "holding type controllable friction damper"), generates friction force by pressing friction materials with actuators. Figure 1 illustrates the mechanism of the holding type controllable friction damper. The relationship between the actuator force and the friction force is expressed by

$$f(t) = \mu p(t) \tag{1}$$

where $f(t)$ is the friction force, μ is the friction coefficient, and $p(t)$ is the Actuator force.

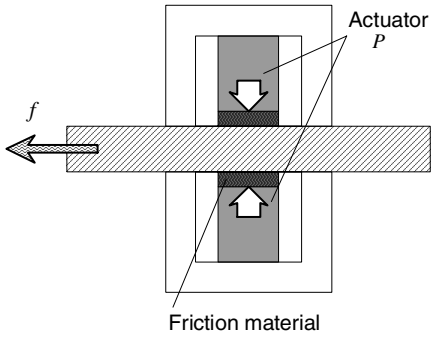

Figure 1 Holding type controllable friction damper

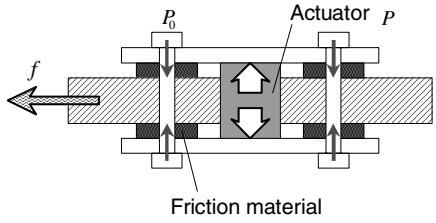

Figure 2 Releasing type controllable friction damper

When static, the actuator force is 0; therefore the friction force is 0. When an earthquake occurs, the damping force of the controllable friction damper is generated by controlling the actuator force. However, if a large earthquake occurs, the power source to the drivers of the controllable friction damper's controller and the actuators may be cut off. In such a case, this damper cannot generate the friction force, and the damping force is 0. The building acts as a low-damping isolation system then because the relative displacement is great and serious damage may occur by collision with surrounding structures.

To solve this problem, a controllable friction damper with a fail-safe mechanism is proposed. Damping force in the proposed damper, (hereafter referred to as "releasing type controllable friction damper"), can be generated in such cases. Figure 2 illustrates the mechanism of the releasing type controllable friction damper. The relationship between the actuator force and the friction force is expressed by

$$f(t) = \mu\big(p_0 - p(t)\big) \tag{2}$$

where $f(t)$ is the friction force, μ is the friction coefficient, p_0 is the initial pressure, and $p(t)$ is the actuator force.

In the initial state, the friction materials are pressed. Once an earthquake occurs, the actuator force is applied to reduce the friction by releasing the pressure between the friction materials. The friction force

can be changed by controlling the actuator force. Even if the controller and the actuators of this damper malfunction and the actuator force $p(t)$ becomes zero, the damping force can be generated by the initial pressure p_0. Therefore, this system can prevent serious damage to the base-isolated structure by preventing collision with surrounding structures when the power supply fails or malfunctions occur.

Analysis model

Figure 3 demonstrates that the seismic isolation system using the controllable friction damper is modeled as a single-degree-of-freedom system. Equations of motion of the model are expressed in two phases, as shown below, considering transition of static/dynamic friction due to the presence or absence of sliding at the friction damper.

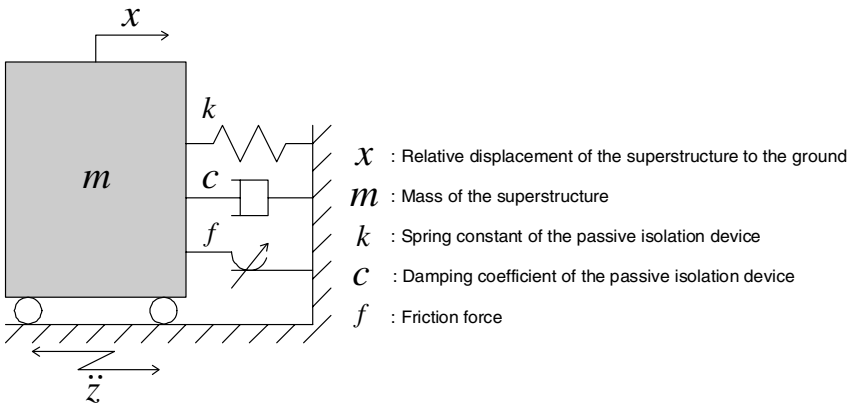

Figure 3 Analysis model

(1) Phase I No sliding at friction damper

$$\begin{cases} x = const. \\ \dot{x} = 0 \\ \ddot{x} = 0 \end{cases} \tag{3}$$

(2) Phase II Sliding at friction damper

$$\ddot{x} + 2\zeta\omega\dot{x} + \omega^2 x + \mathrm{sgn}(\dot{x})F = -\ddot{z} \tag{4}$$

The transition criteria between Phase I and Phase II are:

1) From Phase I to Phase II

$$\left|kx + m\ddot{z}\right| > f \tag{5}$$

2) From Phase II to Phase I

$$\dot{x} = 0 \text{ and } \left|m\ddot{x}\right| < 2f \tag{6}$$

where

$$\zeta = \frac{c}{2\sqrt{mk}} \ , \ \omega = \sqrt{\frac{k}{m}} \ , \ F = \frac{f}{m}$$

Linear quadratic optimum regulator theory

The optimal generation force is obtained by using linear quadratic optimum regulator theory (LQ). A performance index J is defined as follows (assuming that $u = f$):

$$J = \int_0^\infty \left\{ \alpha \left(\ddot{x} + \ddot{z} \right)^2 + \beta x^2 + \gamma u^2 \right\} dt \tag{7}$$

where α, β, and γ are weighting coefficients.

The Linear Quadratic optimal regulator problem is solved, and the optimal control force of u^* is obtained. When semi-active control by the damping force of the controllable friction damper is considered, the direction of force generated by the damper depends on the conditions below.

$$u = \begin{cases} u^* & (u^* \cdot \dot{x} > 0) \\ 0 & (u^* \cdot \dot{x} < 0) \end{cases} \tag{8}$$

The mass of the analysis model is 6,000 kg, the natural period is 3 s, and the damping ratio is 2%. The input seismic waves are EL Centro NS (1940, Imperial Valley Earthquake), JMA NS (1995, Hyogoken-Nanbu Earthquake), Hachinohe NS (1968, Tokachi-Oki Earthquake) and Taft EW (1952, Arvin-Tahachapi Earthquake). The velocity level of the input waves is set to 25 cm/s for each wave. The weighting coefficients of the performance index are selected in the following cases.

Case 1 The response acceleration is smaller (acceleration reduction).
Case 2 Both the response acceleration and the relative displacement are smaller (acceleration and displacement reduction).
Case 3 The relative displacement is smaller (displacement reduction).

Figure 4 shows the results of the simulations by these weighting coefficients in the case of EL Centro NS. For comparison, the results of the passive seismic isolation system with an ideal linear damping factor of 20% are shown in these figures. The maximum input acceleration is also shown in the maximum figures (b) of the response acceleration.

Case 1 is the best in the seismic isolation effect, and the response acceleration is decreased to about 48% on average compared to the passive seismic isolation. Case 3 is the best in the relative displacement reduction performance, and the relative displacement is decreased to about 50% maximum compared to the passive seismic isolation. In Case 2, the response acceleration is decreased to about 64%, and the relative displacement is decreased to about 55% compared to the passive seismic isolation. Therefore, the expected effect is achieved by selecting the weighting coefficients.

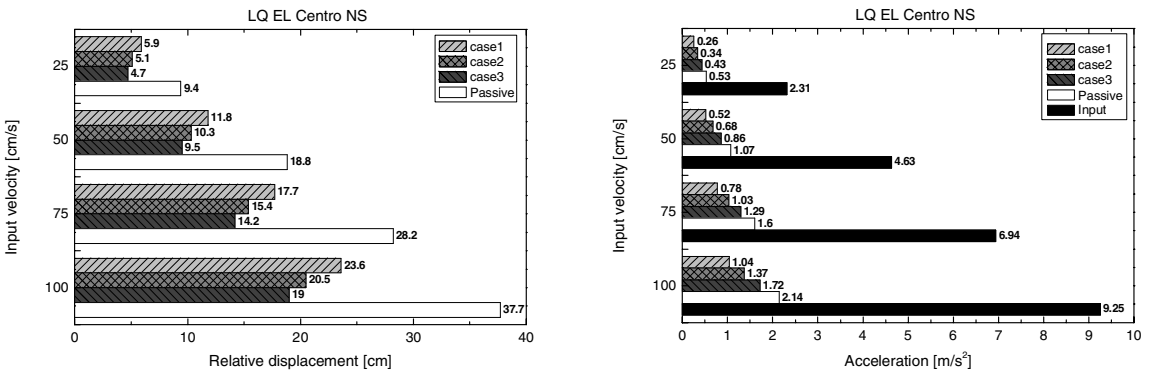

(a) Maximum relative displacement **(b) Maximum response acceleration**

Figure 4 Response simulation results of LQ (EL Centro)

Instantaneous optimal control

When the releasing type controllable friction damper is used, the equation of motion of the seismic isolation system is nonlinear. An Instantaneous Optimal Control algorithm (IOC), which is effective on a nonlinear system, is used to obtain the optimal piezoelectric actuator force $p(t)$. Performance index $J(t)$ of IOC is defined as follows:

$$J(t) = q_v \dot{x}^2(t) + q_d x^2(t) + q_f F^2(t) + p^2(t) \tag{9}$$

where $q_v \geq 0$, $q_d \geq 0$, and $q_f \geq 0$ are weighting coefficients.

The optimal piezoelectric actuator force $p^*(t)$ to minimize the performance function $J(t)$ is obtained as follows:

$$\begin{aligned} p^*(t) = & \frac{q_f \mu^2}{m^2 + q_f \mu^2} p_o \\ & - \frac{q_v m \mu \Delta t \, \mathrm{sgn}(\dot{x}(t))}{2\left(m^2 + q_f \mu^2\right)\left(1 + \frac{\Delta t^2}{6}\omega^2 + \Delta t \zeta \omega\right)} \dot{x}(t) \\ & - \frac{q_d m \mu \Delta t^2 \, \mathrm{sgn}(\dot{x}(t))}{6\left(m^2 + q_f \mu^2\right)\left(1 + \frac{\Delta t^2}{6}\omega^2 + \Delta t \zeta \omega\right)} x(t) \end{aligned} \tag{10}$$

where μ is the friction coefficient and Δt is the sampling time.

The weighting coefficients of performance index are selected in the following cases.

Case 1 The response acceleration is smaller (acceleration reduction).
Case 2 Both the response acceleration and the relative displacement are smaller (acceleration and displacement reduction).
Case 3 The relative displacement is smaller (displacement reduction).

The analytical conditions are the same as in LQ. Figure 5 shows the results of the simulations achieved by these weighting coefficients. For comparison, the results of the passive seismic isolation system with an ideal linear damping factor of 20% are shown in these figures. The maximum input acceleration is also shown in the figures (b) of the maximum response acceleration.

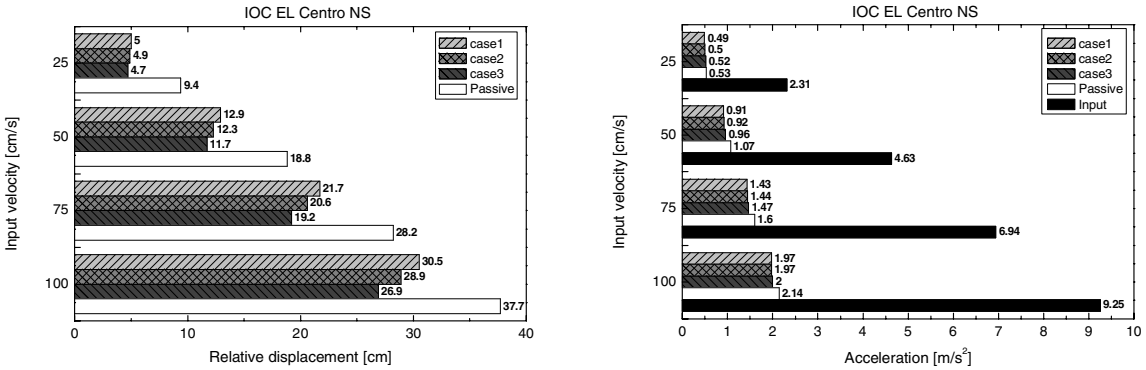

(a) Maximum relative displacement **(b) Maximum response acceleration**

Figure 5 Response simulation results of IOC (EL Centro)

Case 1 is the best seismic isolation. The response acceleration is decreased to about 85% maximum compared to the passive seismic isolation. Case 3 is the best in the displacement reduction performance, and the relative displacement is decreased to about 50% maximum compared to the passive seismic isolation. In Case 2, the response acceleration is decreased to about 90%, and the relative displacement is decreased to about 64% compared to the passive seismic isolation. Therefore, the expected effect is achieved by selecting the weighting coefficients, as it was for the LQ.

Performance during malfunction

To confirm the fail-safe mechanism of the releasing type controllable friction damper, the simulations are executed using a non-functioning actuator. Figure6 shows the results of the simulations for EL Centro NS inputs. For the comparison, the results of the holding type controllable friction damper under the same conditions and the passive seismic isolation system, are also shown in the figures. The holding type controllable friction damper cannot generate the damping force when the actuator doesn't function, and excessive relative displacement occurs. However, the releasing type controllable friction damper generates friction force due to the initial pressure, even if the actuator doesn't function, and relative displacement is not excessive. Moreover, the response acceleration is smaller than the holding type controllable friction damper during the malfunction and is almost the same level as for the passive seismic isolation at high-level inputs. This confirms that the releasing type controllable friction damper is safer than the holding type controllable friction damper.

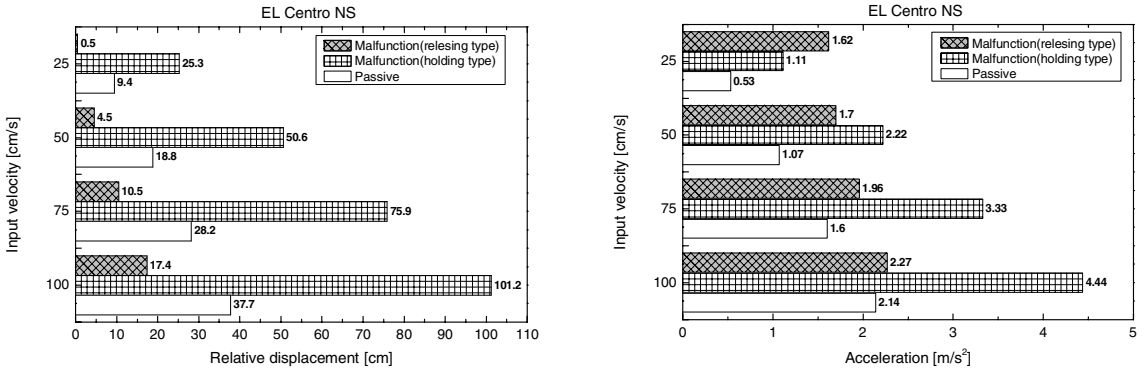

(a) Maximum relative displacement **(b) Maximum response acceleration**

Figure 6 Response simulation results during malfunction (EL Centro)

RELEASING TYPE CONTROLLABLE FRICTION DAMPER

Mechanism

Figure 7 illustrates the drawing and sections of the releasing type controllable friction damper produced for experimental use. The initial pressure p_0 is generated by two pressure bolts, one each on top and bottom of the center. Strain gages are attached on the two pressure bolts and calibrated by a tension test beforehand. They are used as load cells to measure the pressure between the friction materials.

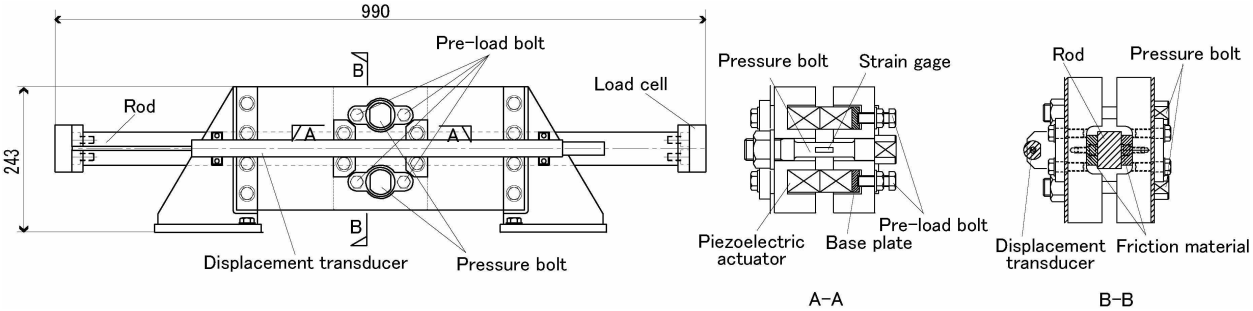

Figure 7 Drawing and sections of the releasing type controllable friction damper

In total, eight piezoelectric actuators are set up in four locations on both sides of these pressure bolts. Therefore, the releasing force is generated with the piezoelectric actuators. Figure 8 shows the piezoelectric actuator [4]. The size is 25x25x36 mm, the maximum driving voltage is 100V, the range displacement is $20\text{x}10^{-6}$m, and the range generation force of the piezoelectric actuator is 20kN. Figure 9 demonstrates the relationship between the generation force and the displacement. Figure 10 demonstrates the relationship between the applied voltage and the displacement. The hysteresis in this relationship is not believed to be a problem in this research.

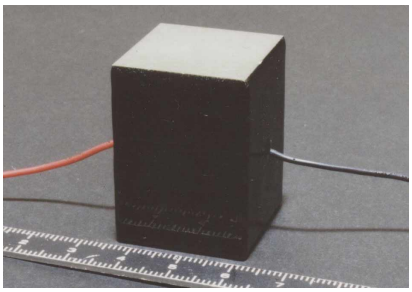

Figure 8 Piezoelectric actuator

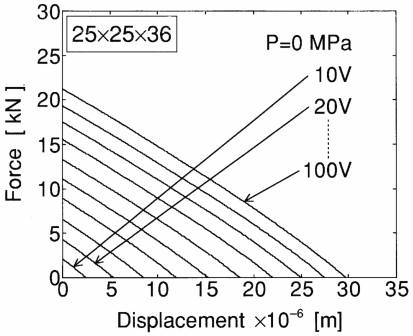

Figure 9 Relationship of generation force and displacement

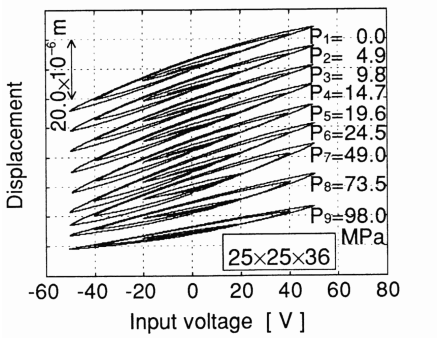

Figure 10 Relationship of applied voltage and displacement

The pre-load of the piezoelectric actuators is adjusted with the pre-load bolts to adjust the generation force and displacement of the piezoelectric actuator.

Characterization experiment

Experimental system

Figure 11 presents the experiment layout, and Figure 12 illustrates the experimental system. The friction damper is excited with the hydraulic actuator set in one side of the rod. The friction force, the displacement, and the releasing force by piezoelectric actuators are measured with the sensors. The driving voltage to the piezoelectric actuators is calculated from the command voltage input to the piezoelectric driver.

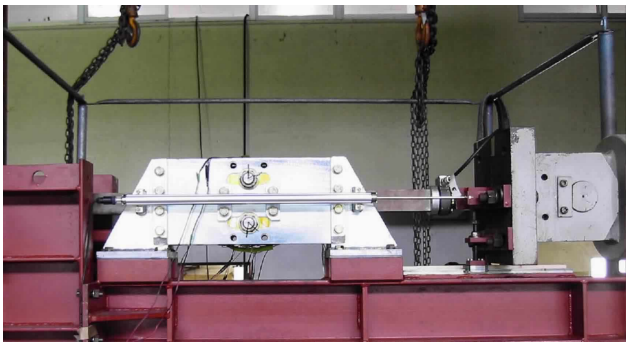

Figure 11 Experiment layout

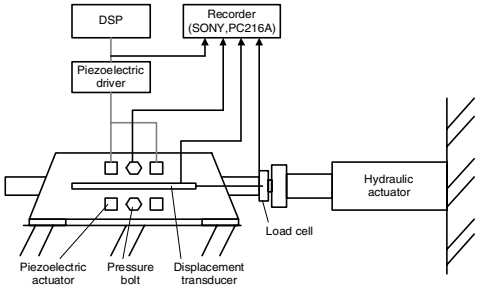

Figure 12 Experiment system

Tests results

To confirm that the friction force isn't dependant on the sliding velocity, tests at four different excitation velocities are conducted when a constant voltage is applied to the piezoelectric actuators. Figure 13 demonstrates the friction force of the damper at each excitation velocity, when 0 V was applied to the piezoelectric actuators. The figure indicates that the friction force is constant, independent of the sliding velocity. 25 V, 50V, and 100V were applied to the piezoelectric actuators, and the pressure between the friction materials changed. Figures 14, 15, and 16 illustrate the results of these tests. Similarly, the friction force is constant, independent of the sliding velocity.

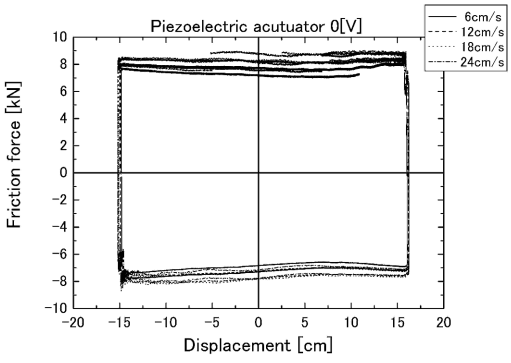

Figure 13 Result of velocity dependence test (0 V applied)

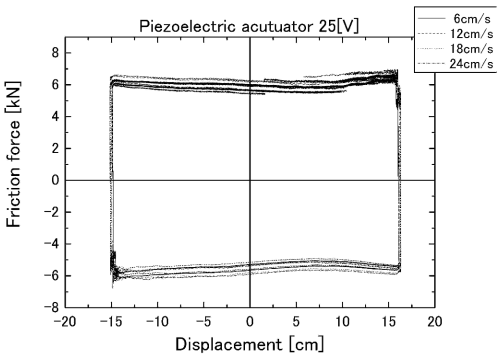

Figure 14 Result of velocity dependence test (25 V applied)

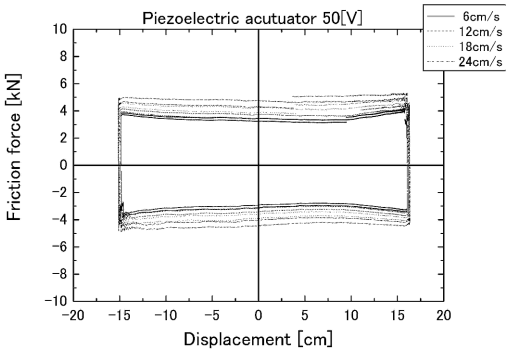

Figure 15 Result of velocity dependence test (50 V applied)

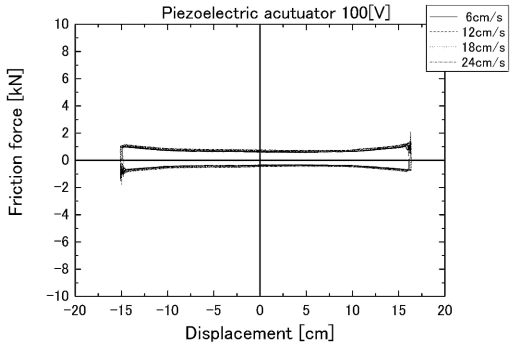

Figure 16 Result of velocity dependence test (100 V applied)

Figure 17 illustrates the relationship between the voltage applied to the piezoelectric actuators and the friction force of the damper when the sinusoidal voltage applied to the piezoelectric actuators was changed from 0V to 100V. Hysteresis and nonlinearity exist in the relationship between the applied voltage and the friction force. This hysteresis is related to the hysteresis of the piezoelectric actuators. The nonlinearity is an influence of the saturation of the minimum friction force. However, this relationship is approximated as a linear function for simplification. The approximated linear function is

$$f = 2.97 - 0.0312E \tag{11}$$

where f is the friction force of the controllable friction damper of releasing type [kN] and E is the voltage applied to the piezoelectric actuators [V].

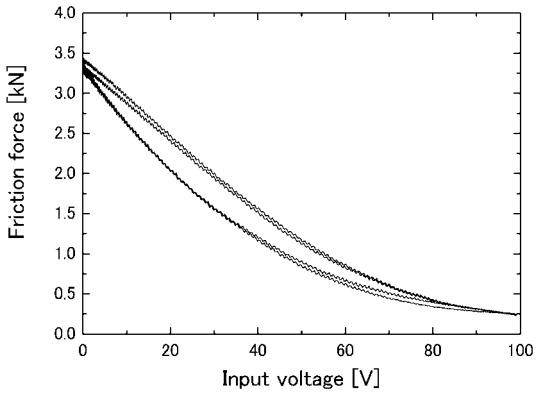

Figure 17 Applied voltage and friction force relationship

SHAKE TABLE TEST FOR SEMI-ACTIVE SEISMIC ISOLATION SYSTEM

Base-isolation building model

The building model used for the tests consists of a steel skeleton frame and steel plate weights, and is supported by four linear bearings. Figure 18 depicts the test building model. The superstructure and base frame are connected with coil springs and the releasing type controllable friction damper. The total mass of the superstructure is 6350 kg. The first mode natural frequency of the isolation system is 0.33 Hz.

Control system

The control system consists of sensors, DSP, A/D-D/A converters, and a piezoelectric driver. The control voltage calculated by DSP is input into the piezoelectric driver. Figure 19 illustrates the control system.

Figure 18 Test building model

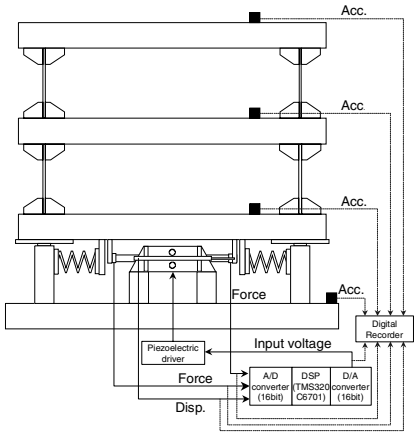

Figure 19 Control system

Test result

Figure 20 illustrates the relative displacement and the response acceleration for the EL Centro NS inputs when semi-active isolation controller is designed by LQ. Acceleration is smaller in LQ-1 and relative displacement is smaller in LQ-2. 'P-1' and 'P-2' in the figures indicate passive seismic isolation using a friction damper with a constant pressure. In case P-1 (P-2), the pressure is set to begin to slide the friction damper if the input acceleration exceeds 10cm/s^2 (25cm/s^2).

Comparing LQ-1 with P-1, the response acceleration is almost the same, but the relative displacement of LQ-1 is decreased to about 60%. Additionally, comparing LQ-2 with P-2, the relative displacement is almost the same, but the response acceleration of LQ-2 decreased to about 60%. The expected effects are thus achieved in both LQ cases.

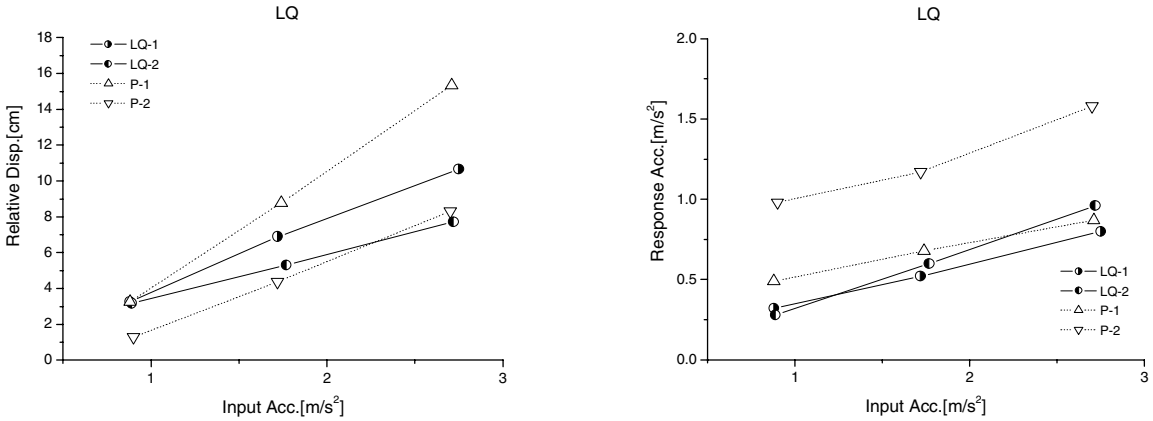

Figure 20 Relative displacement and response acceleration of LQ

Figure 21 depicts the result of the IOC test. Acceleration is smaller in IOC-1 and relative displacement is smaller in IOC-2. These figures also show the results of the passive seismic isolation.

Compared to P-1, the relative displacement of IOC-1 decreases to about 76% and 47% in IOC-2. The response acceleration of IOC-2 and P-1 is almost the same. However, the response acceleration of IOC-1 is smaller than that of IOC-2 and P-1. Compared to P-2, the response acceleration of IOC-1 decreases to about 50%, and to 55% in IOC-2. The expected effects are achieved in IOC as well as LQ.

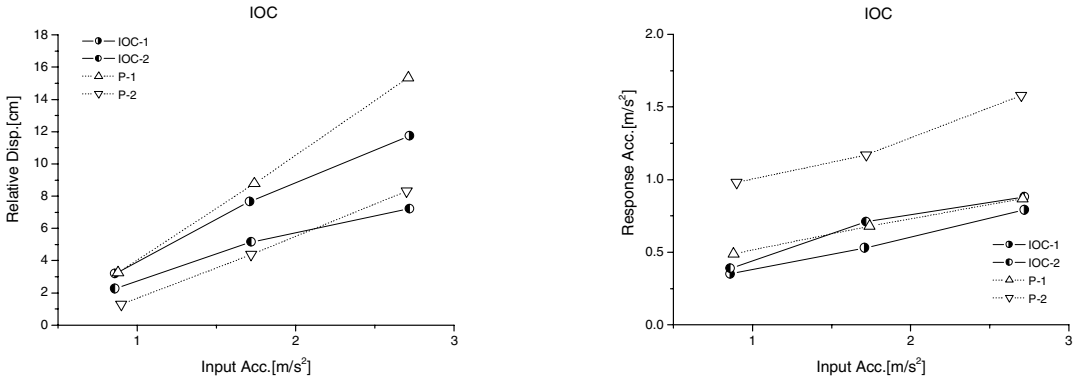

Figure 21 Relative displacement and response acceleration of IOC

Figure 22 illustrates the time-histories in LQ-1, IOC-1 and P-1. The input is EL Centro NS of 300cm/s^2. These figures also show the simulation results. The simulation results agree with experiment results as well, confirming that the analysis model is valid.

CONCLUSIONS

A new controllable friction damper with a fail-safe mechanism is produced, and numerical simulations of the semi-active seismic isolation system with this controllable friction damper whose controller was designed from LQ and IOC were conducted. The seismic isolation effects and the relative displacement reduction effects of semi-active seismic isolation system damper improved in comparison with the passive seismic isolation system. The anticipated effects were achieved by selecting the weighting coefficients in each control rule of LQ and IOC. Moreover, even if the controller and the actuator of the controllable friction damper don't function when a large earthquake occurs, the semi-active seismic isolation system using the releasing type controllable friction damper can prevent excessive displacement because of its fail-safe mechanism. Therefore, it is confirmed that the releasing type controllable friction damper is safer than the holding type controllable friction damper.

Characterization experiments for the releasing type controllable friction damper using the piezoelectric actuators were conducted. It was experimentally confirmed that the friction force of the releasing type controllable friction damper can be changed by controlling the piezoelectric actuator force. A numerical model of this friction damper was subsequently developed.

Shaking table tests for a semi-active isolation system with this damper were conducted. The tests confirmed that the semi-active seismic isolation system using this friction damper performs better than the passive seismic isolation system.

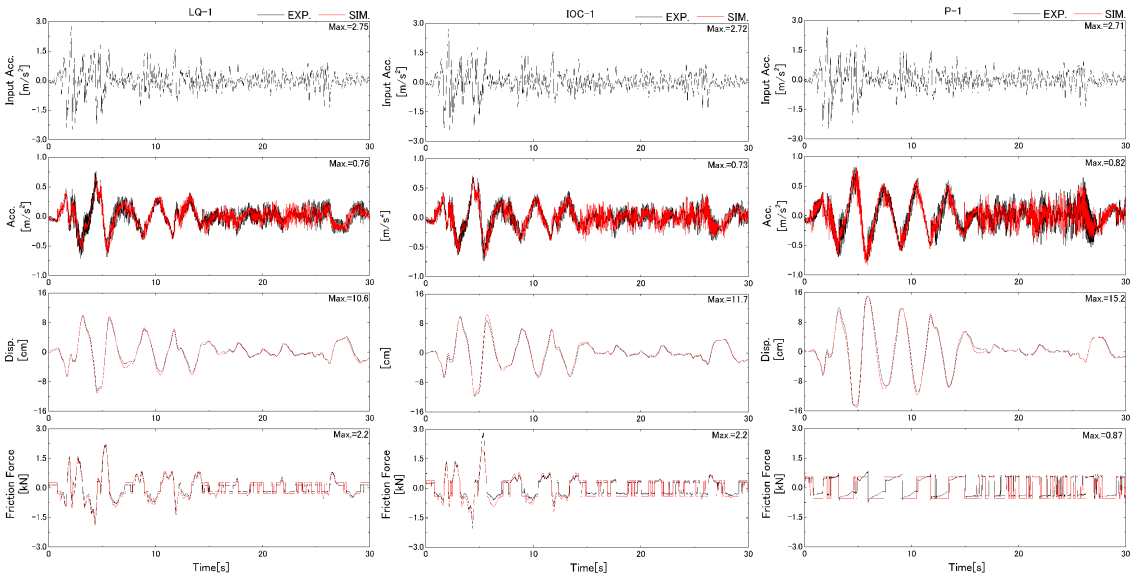

Figure 22 Time histories of responses of semi-active and passive systems (Experimental and simulation results)

REFERENCES

1. Fujita T. “Research, development and application of seismic isolation systems in Japan”, Proceeding of the International Meeting on Earthquake Protection of Builgings, Italy, 6-8, June, 1991,77/C-90/C.
2. Fujita T., Kabeya K., Hayamizu Y., Aizawa S., Higashino M., Kubo T., Haniuda N., and Mori T., “Semi-active seismic isolation system using controllable friction damper (1st report, Development of controllable friction damper and fundamental study of semi-active control system)”, Trans. of Japan Soc. Mech. Eng.,1991, 57, 536 Ser.C, 1122-1128(in Japanese).
3. Fujita T., Shimazaki M., Hayamizu Y., Aizawa S., Higashino M., Kubo T., and Haniuda N., “Semi-active seismic isolation system using controllable friction damper (2nd report, Study of the system with distributed controllable friction dampers)”, Trans. of Japan Soc. Mech. Eng.,1992, 58, 551 Ser.C, 2012-2016(in Japanese).
4. Shimazaki M Fujita T., “Experimental study of piezoelectric actuator for large-scale smart structure (2nd report, actuator characteristics of 25x25x36 piezoelectric actuator of stack type)”, Bimonthly journal of Institute of Industrial Science, University of Tokyo, 1996, 49, 9, 449-452(in Japanese).